Role of single-ion excitations in the mixed-spin quasi-one-dimensional quantum antiferromagnet Nd_2BaNiO_5

A. Zheludev and S. Maslov
Department of Physics, Brookhaven National Laboratory, Upton, New York 11973

T. Yokoo and J. Akimitsu
Department of Physics, Aoyama-Gakuin University, 6-16-1 Chitosedai, Setagaya-ku, Tokyo 157 Japan

S. Raymond
Université de Geneve DPMC 24, quai Ernest Ansermet 1211, Geneve 4, Switzerland

S. E. Nagler
Oak Ridge National Laboratory, Building 7692, MS 6393, P.O. Box 2008, Oak Ridge, Tennessee 37831

K. Hirota
Department of Physics, Tohoku University, Aramaki, Aoba-ku, Sendai 980-8578, Japan
(Received 21 October 1999)

Inelastic neutron scattering experiments on Nd_2BaNiO_5 single crystals and powder samples are used to study the dynamic coupling of one-dimensional Haldane-gap excitations in the $S=1$ Ni^{2+}-chains to local crystal-field transitions, associated with the rare earth ions. Substantial interference between the two types of excitations is observed even in the one-dimensional paramagnetic phase. Despite that, the results provide solid justification for the previously proposed ''static staggered field'' model for R_2BaNiO_5 nickelates. The observed behavior is qualitatively explained by a simple chain-random-phase-approximation model.

I. INTRODUCTION

Linear-chain rare earth nickelates with the general formula R_2BaNiO_5 were recently recognized as unique model compounds for experimental studies of Haldane-gap quantum spin chains in strong *staggered* applied fields.[1] In these materials the Haldane subsystem is formed by chains of $S=1$ Ni^{2+} ions with relatively strong, almost isotropic, nearest-neighbor antiferromagnetic (AF) exchange interactions ($J\approx 27$ meV). The corresponding Haldane energy gap in the magnetic excitation spectrum is $\Delta\approx 11$ meV.[2–7] An effective staggered exchange field H_π acting on these one-dimensional (1D) objects is generated by three-dimensional (3D) magnetic long-range ordering in the ''auxiliary'' sublattice of magnetic rare earth ions, which typically occurs at Néel temperatures of several tens of kelvin.[8] The magnitude of the staggered field is proportional to the ordered moment on the R^{3+} sites, and can be varied in an experiment, by changing the temperature. Static magnetic properties of R_2BaNiO_5 compounds are rather well described by the chain-mean-field (MF) model.[9,6] Using this theory to analyze the measured temperature dependences of magnetic order parameters for a number of R_2BaNiO_5 species previously enabled us to extract the *staggered magnetization function* for a single Haldane spin chain.[9] These experimental results were found to be in excellent agreement with theoretical calculations for isolated chains.[10,11] The view of R_2BaNiO_5 systems as Haldane spin chains immersed in a static staggered field (SSF) model turned out to be successful in describing the behavior of Haldane-gap excitations as well.[10,6] In agreement with analytical[10,12] and numerical[11] predictions, the energy gap was shown to increase quadratically with H_π in Pr_2BaNiO_5, Nd_2BaNiO_5, and $(Nd_xY_{1-x})_2BaNiO_5$ systems in their magnetically ordered phases.

The focus of the present paper is on a different, potentially very important, aspect in the magnetism of R_2BaNiO_5 materials, namely, on the strong spin-orbit interactions typically associated with rare earth ions. Of particular interest are local (single-ion) crystal-field (CF) excitations of the rare earths and their possible interactions with the Haldane-gap modes propagating on the Ni chains. Until now this effect has not been investigated in sufficient detail. The models used for R^{3+} in R_2BaNiO_5 were in most cases restricted to considering the ion's lowest-energy electronic configurations: effective $S=1/2$ doublets for Kramers ions like Nd^{3+} or Er^{3+} (Ref. 9) or singlets for Pr^{3+} (Ref. 3). Higher-energy electronic states were entirely ignored. Yet, in a number of materials, particularly in Nd_2BaNiO_5,[4] several CF transitions occur very close to the Haldane-gap energy. In this situation a strong coupling between the two types of excitations can be expected. Does this interaction limit the applicability of the SSF model? Does it give rise to peculiar ''mixed'' Ni-R excitations? If so, do these ''mixed'' modes retain a predominantly 1D character of Haldane-gap excitations? In the present paper we address these important and interesting questions in a series of inelastic neutron scattering measurements on Nd_2BaNiO_5.

II. EXPERIMENT

The crystal structure of R_2BaNiO_5 compounds is discussed in detail elsewhere.[13] Nd_2BaNiO_5 crystallizes in an

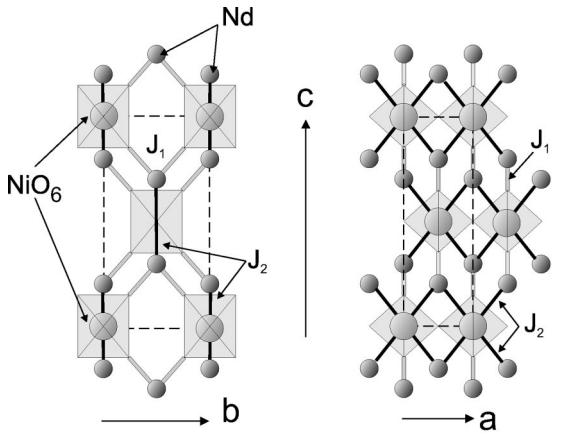

FIG. 1. A schematic representation of the magnetic interaction geometry in the structure of R_2BaNiO_5.

orthorhombic unit cell, space group *Immm*, $a \approx 3.8$ Å, $b \approx 5.8$ Å, and $c \approx 11.7$ Å.[5] The $S=1$ Ni chains are formed by orthorhombically distorted NiO_6 octahedra that are lined up in the (100) crystallographic direction, sharing their apical oxygen atoms. The Nd sites are positioned in between these chains, linking nearest-neighbor chains along the crystallographic *b* axis (Fig. 1). We shall denote the corresponding exchange constant as J_1. In addition, one can expect substantial coupling of each Nd^{3+} ion to two Ni^{2+} sites in a third nearby chain (exchange constant J_2). The site symmetry for the rare earth ions is sufficiently low, and the electronic ground state for Nd^{3+} is a Kramers doublet. The Néel temperature for Nd_2BaNiO_5 is $T_N=48$ K. The magnetic structure is as described in Ref. 8 and 14.

The simplest technique used to locate CF excitations is inelastic neutron scattering on powder samples. Such measurements were previously performed on Nd_2BaNiO_5 for energy transfers up to 30 meV using a three-axis spectrometer.[4] To learn about higher-energy CF transitions we carried out preliminary experiments on the time-of-flight (TOF) spectrometer LAM-D, installed at the spallation neutron source KENS in the High Energy Accelerator Research (KEK). LAM-D implements the so-called inversion geometry and is equipped with four fixed PG crystal analyzers. The measured spectra are automatically *Q* integrated in a certain momentum range that roughly corresponds to 1–2 $Å^{-1}$ at $\hbar\omega=0$. Energy transfers from -2 meV to 200 meV are accessible. The energy resolution at the elastic scattering position is about 300 μeV and the relative resolution $\delta(\hbar\omega)/\hbar\omega$ is fairly constant, around 4%, between $\hbar\omega=2$ and 60 meV. In the experiment we used roughly 10 g of Nd_2BaNiO_5 powder prepared by the solid-state reaction method. The sample environment was a standard closed-cycle refrigerator.

Most of the data presented below were obtained on single-crystal samples. These experiments were carried out at the High Flux Isotope Reactor (Oak Ridge National Laboratory) on the HB-1 triple-axis spectrometer. We used the same assembly of three coaligned single crystals as in previous studies.[6] The sample was in all cases mounted with the $(h,k,0)$ reciprocal-space plane parallel to the scattering plane of the spectrometer, to compliment previous $(h,0,l)$ measurements. A neutron beam of 14.7 meV or 30.5 meV fixed final energy of 30.5 meV fixed incident energy was used

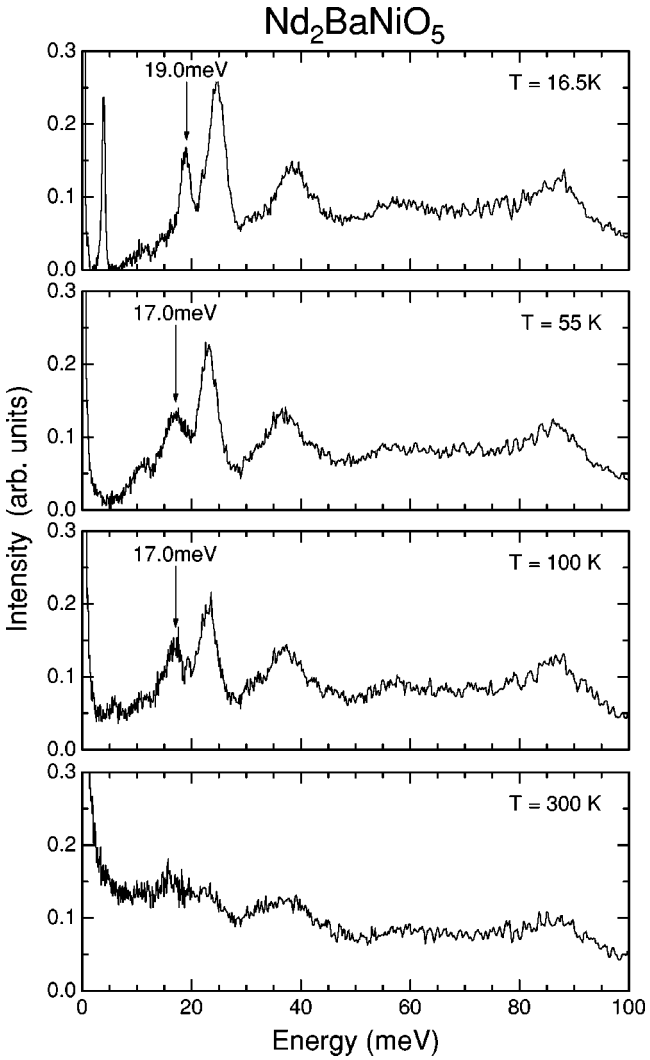

FIG. 2. LAM-D inelastic spectra measured in Nd_2BaNiO_5 powder samples at different temperatures. The contribution of the sample holder has been subtracted.

with 60′-40′-40′-120′ collimations and a pyrolitic graphite (PG) filter positioned after the sample. PG (002) reflections were used for monochromator and analyzer. The measurements were done with energy transfers up to 35 meV. The sample environment was a standard Displex refrigerator, and the temperature range 35–65 K was explored. The growth directions of the crystals roughly coincide with the (100) crystallographic axis. In the experiment the crystal rods were therefore positioned horizontally in the scattering plane. In this geometry absorption effects, primarily due to the presence of Nd nuclei, may be substantial, as will be discussed in detail below.

III. RESULTS

A. Powder data

Inelastic powder experiments, while obviously less informative than single-crystal measurements, provide a convenient view of the excitation spectrum in a wide energy range. Figures 2(a)–2(d) show the measured inelastic spectra for Nd_2BaNiO_5 powder at $T=16.5$, 55, 100, 300 K, respectively. The background originating from the sample holder

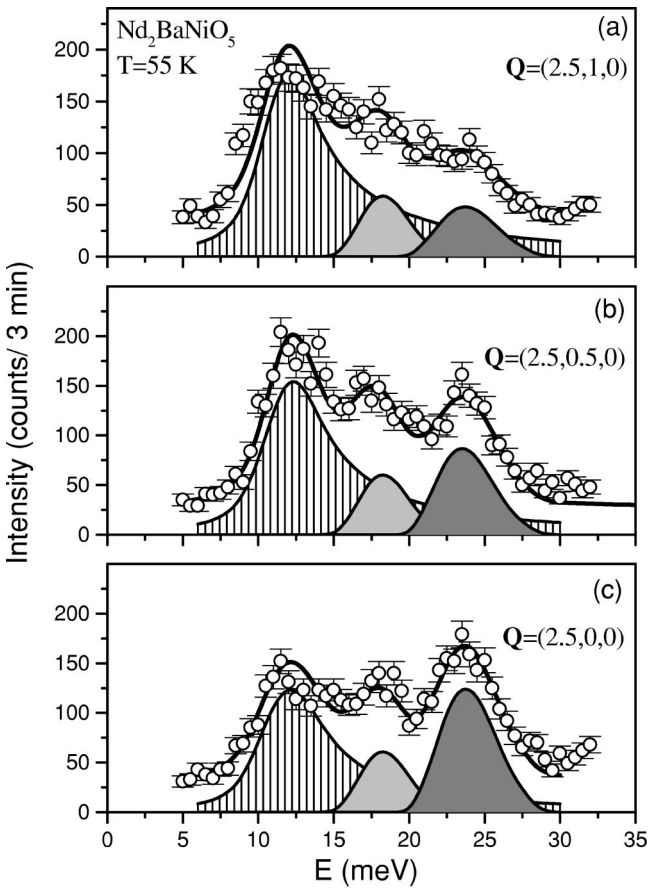

FIG. 3. Typical constant-Q scans measured in Nd_2BaNiO_5 at $T=55$ K at the 1D AF zone center $h=2.5$, at different momentum transfers perpendicular to the chain axis (symbols). The solid lines are a global fit to the model cross section, as described in the text. The hatched, light-gray, and gray peaks represent partial contributions from the Haldane-gap and two crystal-field excitations, respectively.

was measured separately and subtracted from the data sets shown. Each scan corresponds to 16–20 h of counting time. At $T=55$ K, above the Néel temperature $T_N=48$ K, one clearly sees at least three features that are likely to be Nd-CF excitations [Fig. 2(b)]. In addition to the two previously identified low-energy modes at $E_1=18$ meV and $E_2=24$ meV energy transfer,[4] a broad yet intense peak is seen at 40 meV. As in previous three-axis powder measurements, at 11 meV one can also see a shoulder corresponding to Haldane excitations. The latter are known to have a steep dispersion along the chain axis. As a result, compared to the dispersionless CF excitations, the Ni-chain modes appear substantially weakened in a powder experiment, as opposed to single-crystal measurements. No substantial scattering is seen within the Haldane gap. At $T=100$ K the 11 meV shoulder is much less pronounced, while the CF peaks remain almost unchanged [Fig. 2(c)]. As could be expected, at high temperatures the entire spectrum becomes smeared out [Fig. 2(d)].

A drastic change in the spectrum occurs upon cooling through the Néel temperature [Fig. 2(a), $T=16.5$ K]. An intense resolution-limited peak emerges inside the gap and is centered at 4 meV energy transfer. This feature corresponds to a dispersionless Ising-like spin wave associated with long-range magnetic ordering.[6] Below $T=20$ K the Haldane gap was previously shown to exceed 15 meV.[6] In apparent contradiction with this single-crystal result, the 11 meV shoulder is weakened but still visible in our new 16.5 K powder data. One possible explanation of this is that the shoulder is partially due to a weak, previously unobserved CF excitation: at low temperatures the Haldane gap increases, but the new CF mode stays at 11 meV energy transfer. Some of the single-crystal results presented below support this interpretation.

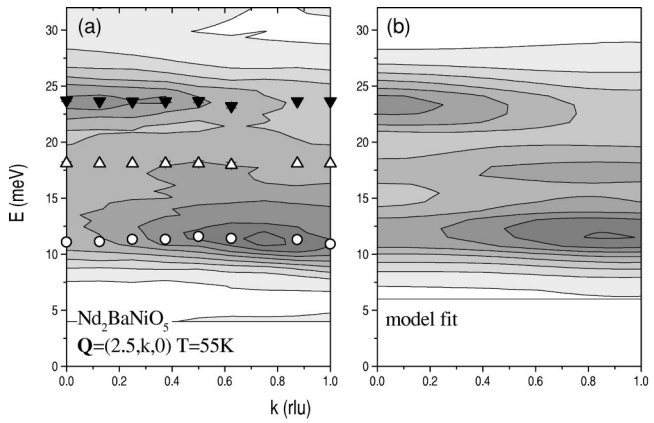

FIG. 4. (a) Contour plot of inelastic scattering intensity measured in Nd_2BaNiO_5 at $T=55$ K at the 1D AF zone center $h=2.5$ in a series of constant-Q scans (20 counts/3 min contour steps). The symbols show the energies of Haldane (circles) and two crystal-field excitations (triangles), as determined from fitting a model cross section to individual scans. (b) The result of a global fit to the data shown in (a).

A more complete, quantitative, analysis of the powder data is not presently possible, as the phonon background is not known. In the future we plan to supplement these data with ''background'' measurements on Y_2BaNiO_5, to isolate the magnetic contribution of the rare earth ions in Nd_2BaNiO_5. For the purpose of the present paper, however, we can draw one useful conclusion: in trying to understand the coupling of the Ni and Nd subsystems on energy scales comparable to Δ, we can safely restrict ourselves to considering the two strong CF excitations at 18 meV and 24 meV only.

B. Transverse intensity modulation

1. Constant-Q scans

Having verified the location of major CF excitations in powder measurements, we proceeded with more detailed single-crystal experiments. As a first step, we investigated the b-axis dependence of intensities and energies for the Ni-chain and Nd-CF excitations near the 1D AF zone center. Typical constant-Q scans collected at $\boldsymbol{Q}=(0,k,2.5)$, for several values of k, are shown in Fig. 3. A total of nine scans of this type were measured, with k ranging from 0 to 1, at $T=55$ K (just above the temperature of magnetic ordering, $T_N=48$ K). These data are summarized in the intensity-contour plot in Fig. 4(a). Peaks corresponding to the Ni-chain excitations and to the two CF modes are clearly seen. The central result of this work is that *the relative intensities of these excitations appear to vary significantly with transverse momentum transfer*.

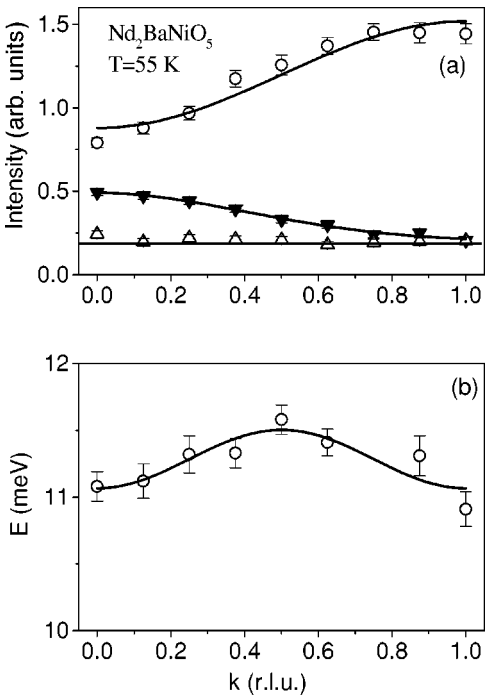

FIG. 5. (a) k dependence of excitation intensities measured in Nd_2BaNiO_5 at $T=55$ K, as deduced from model cross section fits to individual const-Q scans [see Fig. 4(a)]. (b) k dependence of Haldane-gap energy, determined in the same fashion. Solid lines are guides for the eye.

To better understand this intensity variation and to look for a transverse dispersion in any of the three modes, we analyzed each of the measured const-Q scans using a semiempirical parameterized model cross section:

$$S(\boldsymbol{Q},\omega)=S_H(\boldsymbol{Q},\omega)+S_1(\boldsymbol{Q},\omega)+S_2(\boldsymbol{Q},\omega), \tag{1}$$

$$S_H(\boldsymbol{Q},\omega)=S_H^{(0)}\frac{\Delta^2}{\Gamma}\frac{1}{(\hbar\omega)^2+\Delta^2(\hbar\omega-\hbar\omega_{\boldsymbol{Q}})^2/\Gamma^2}[f_{\mathrm{Ni}}(Q)]^2, \tag{2}$$

$$S_1(\boldsymbol{Q},\omega)=S_1^{(0)}\delta(\hbar\omega-E_1)[f_{\mathrm{Nd}}(Q)]^2, \tag{3}$$

$$S_2(\boldsymbol{Q},\omega)=S_2^{(0)}\delta(\hbar\omega-E_2)[f_{\mathrm{Nd}}(Q)]^2, \tag{4}$$

$$(\hbar\omega_{\boldsymbol{Q}})^2=\Delta^2+v^2\sin^2(Q_{\parallel}a). \tag{5}$$

In these equations $S_H(\boldsymbol{Q},\omega)$, $S_1(\boldsymbol{Q},\omega)$, and $S_2(\boldsymbol{Q},\omega)$ are the partial contributions of the Haldane-gap and two CF modes, respectively. The coefficients $S_H^{(0)}$, $S_1^{(0)}$, and $S_2^{(0)}$ represent the intensities of each component. The spin wave velocity $v=6.07\Delta$ (Ref. 15) and intrinsic energy width Γ characterize the Haldane-gap excitations. In our analysis Γ was fixed to a value of 1 meV, as in previous studies.[6] $Q_{\parallel}$ is the projection of the scattering vector onto the chain axis. Finally, $f_{\mathrm{Ni}}(Q)$ and $f_{\mathrm{Nd}}(Q)$ are magnetic form factors for Ni^{2+} and Nd^{3+} ions. The data analysis was performed assuming seven independent parameters: the three intensity prefactors, a constant background, and the three characteristic energies Δ, E_1, and E_2. The cross section was convoluted with the spectrometer resolution function and fit separately to each scan. Typical fits are shown in solid lines in Fig. 3. This analysis yielded a

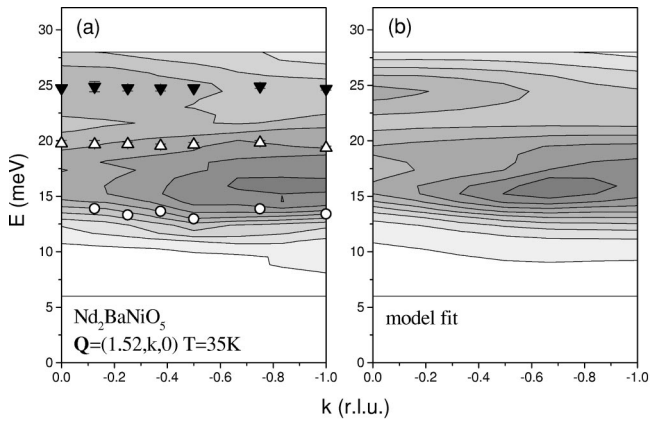

FIG. 6. (a) Contour plot of inelastic scattering intensity measured in Nd_2BaNiO_5 at $T=35$ K at the 1D AF zone center $h=1.5$ in a series of constant-Q scans (20 counts/3 min contour steps). The symbols show the energies of Haldane (circles) and two crystal-field excitations (triangles), as determined from fitting a model cross section to individual scans. (b) The result of a global fit to the data shown in (a).

measurement of the b-axis dispersion relation in each branch, plotted with symbols in Fig. 4(a). To within experimental error the CF branches appear flat, and only a very small dispersion is seen in the Haldane modes [Fig. 5(b)]. The Haldane-gap energy is a maximum at the transverse zone boundary $k=0.5$. The intensity variation for each mode is shown in Fig. 5(a). The intensity of the 18 meV excitation appears almost k independent. At the same time, intensities of both the Haldane and the 24 meV CF modes are strongly k dependent, and are seemingly in ''antiphase'' one to another.

Data sets similar to those described above were also collected at $T=35$ K, i.e., below the Néel temperature. These results are summarized in Figs. 6 and 7. Compared to the high-temperature measurements, the Haldane-gap energy is increased to about 14 meV. The Haldane branch thus occurs closer to the 18 meV CF mode. It is also almost twice as weak as at $T=55$ K. As a result, the scattering of data points in the measured transverse dispersion curve shown in Fig. 7(b) is rather large, and the bandwidth cannot be reliably determined. Compared to the high-temperature regime, the magnitude of intensity variations in the both the Haldane and 24 meV excitations are visibly reduced [see Fig. 7(a)].

2. Global fits to data

The final analysis of the measured constant-Q scans was performed by fitting a model cross section simultaneously to all data collected at each temperature [Figs. 4(a) and 6(a)]. Formulas 1–5 used to analyze individual scans were modified to allow for a transverse dispersion and intensity modulation in each branch. The appropriate forms for these k dependences are derived in the theory section below. The corresponding expression for the magnetic dynamic structure factor near the 1D AF zone center is as follows:

$$S(\boldsymbol{Q},\omega)=S_H(\boldsymbol{Q},\omega)+S_1(\boldsymbol{Q},\omega)+S_1(\boldsymbol{Q},\omega), \tag{6}$$

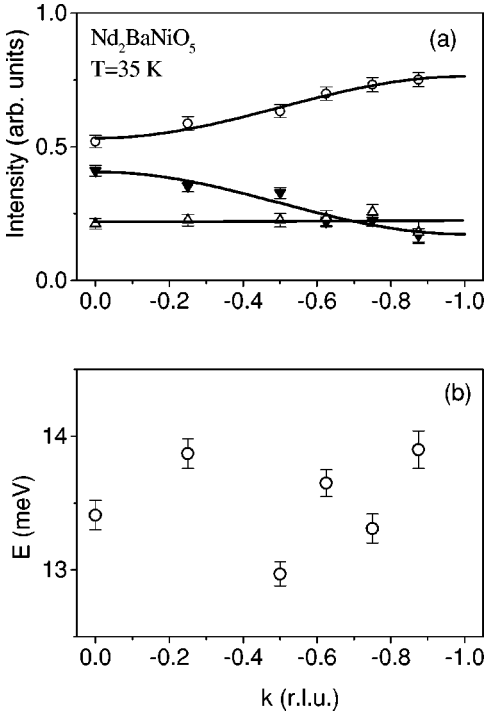

FIG. 7. (a) k dependence of excitation intensities measured in Nd_2BaNiO_5 at $T=35$ K, as deduced from model cross section fits to individual const-Q scans [see Fig. 6(a)]. (b) k dependence of Haldane-gap energy, determined in the same fashion. Solid lines are guides for the eye.

$$S_H(\boldsymbol{Q},\omega)=S_H^{(0)}\frac{\Delta^2}{\Gamma}\frac{1}{(\hbar\omega)^2+\Delta^2(\hbar\omega-\hbar\omega_{\boldsymbol{Q}})^2/\Gamma^2}\{[f_{\mathrm{Ni}}(Q)]^2 + A_H(f_{\mathrm{Ni}}(Q)f_{\mathrm{Nd}}(Q))\cos(Q_\perp b/2)\}, \quad (7)$$

$$S_1(\boldsymbol{Q},\omega)=S_1^{(0)}\delta(\hbar\omega-E_1(Q_\perp))\{[f_{\mathrm{Nd}}(Q)]^2 + A_1(f_{\mathrm{Ni}}(Q)f_{\mathrm{Nd}}(Q))\cos(Q_\perp b/2)\}, \quad (8)$$

$$S_2(\boldsymbol{Q},\omega)=S_2^{(0)}\delta(\hbar\omega-E_2(Q_\perp))\{[f_{\mathrm{Nd}}(Q)]^2 + A_2(f_{\mathrm{Ni}}(Q)f_{\mathrm{Nd}}(Q))\cos(Q_\perp b/2)\}, \quad (9)$$

$$(\hbar\omega_{\boldsymbol{Q}})=\sqrt{\Delta^2+v^2\sin^2(Q_\parallel a)}+B_H\cos^2(Q_\perp b/2), \quad (10)$$

$$E_1(Q_\perp)=E_1+B_1\cos^2(Q_\perp b/2), \quad (11)$$

$$E_2(Q_\perp)=E_2+B_2\cos^2(Q_\perp b/2). \quad (12)$$

In these equations $Q_\perp$ is the component of momentum transfer parallel to the b axis. As explained in the theory section, the dimensionless coefficients A_H, A_1, and A_2 quantify the admixture of Nd-CF spin fluctuations to the chain modes and vice versa. B_H, B_1, and B_2 are respective magnitudes of transverse dispersion. To minimize the number of adjustable parameters the values $B_1\equiv 0$, $A_2\equiv 0$ (no dispersion observed), and $A_1\equiv 0$ (the mode appears not to be modulated) were fixed, which hardly affected the final χ^2. The results of the global least-squares fitting to the $T=55$ K and $T=35$ K data are shown in Figs. 4(b) and 6(b), respectively. The refined values of all parameters are summarized in Table I. In both cases a $\chi^2=1.7$ was achieved, which suggests that the model cross section describes the observed behavior reasonably well. As discussed above, the coefficients for intensity modulations in all three modes, as well as the dispersion bandwidth for the Haldane branch at $T=55$ K, determined in this analysis, can be considered rather reliable. On the contrary, the large value for B_H at $T=35$ K is somewhat suspect. In the refinement this parameter has a strong correlation with E_1; i.e., the Haldane gap is not very well resolved. This also accounts for the large scattering in the points obtained in fits to individual scans in Fig. 7(b). There is little doubt, however, that the bandwidth of transverse dispersion remains very small even in the magnetically ordered state.

TABLE I. Parameters characterizing the transverse dispersion and intensity modulation of the Haldane-gap and crystal-field excitations in Nd_2BaNiO_5, as obtained from global fits of a model cross section to series of constant-Q scans.

	$T=55$ K, $\boldsymbol{Q}=(2.5,k,0)$	$T=35$ K, $\boldsymbol{Q}=(1.52,k,0)$
Δ (meV)	10.97 (0.09)	13.26 (0.07)
A_H	−0.17 (0.01)	−0.12 (0.02)
B_H (meV)	−0.19 (0.14)	0.64 (0.15)
$S_H^{(0)}$ (arb. units)	1.17 (0.03)	0.66 (0.02)
E_1 (meV)	18.33 (0.09)	19.7 (0.1)
A_1	0 (fixed)	0 (fixed)
B_1 (meV)	0 (fixed)	0 (fixed)
$S_1^{(0)}$ (arb. units)	0.20 (0.01)	0.22 (0.02)
E_2 (meV)	23.8 (0.06)	24.6 (0.09)
A_2	0.72 (0.06)	0.37 (0.05)
B_2 (meV)	0 (fixed)	0 (fixed)
$S_2^{(0)}$ (arb. units)	0.34 (0.01)	0.30 (0.01)

3. Wide-range constant-E scans

It is implied in Eqs. (7)–(9) that the intensity modulation in all modes is periodic along the b axis. To verify this periodicity we performed constant-E scans at the Haldane gap energy and at $\hbar\omega=25$ meV, covering a broad range of transverse momentum transfers. Typical raw data collected at $T=55$ K are shown in Figs. 8(a) and 9(a). A serious technical problem with such measurements is that they are strongly influenced by neutron absorbtion in the sample. In each scan k varies significantly at a constant value of h. As a result, the crystal rods rotate relative to the incident and outgoing beams by a large angle. Absorbtion corrections could be calculated, but additional undesirable effects arising from the size (length) of the sample, being comparable to the width of the incident neutron beam, are difficult to account for analytically. To correct the data for any transmission effects, we measured the actual transmission coefficient *in situ*. This was done separately for each point of the constant-E scans performed. The monochromator, sample, and scattering angles of the spectrometer were set to values calculated for a given point in the inelastic scan. The analyzer angles were then set to the elastic position to measure the intensity of incoherent scattering. Incoherent scattering being isotropic, the measured incoherent intensity can be assumed to be

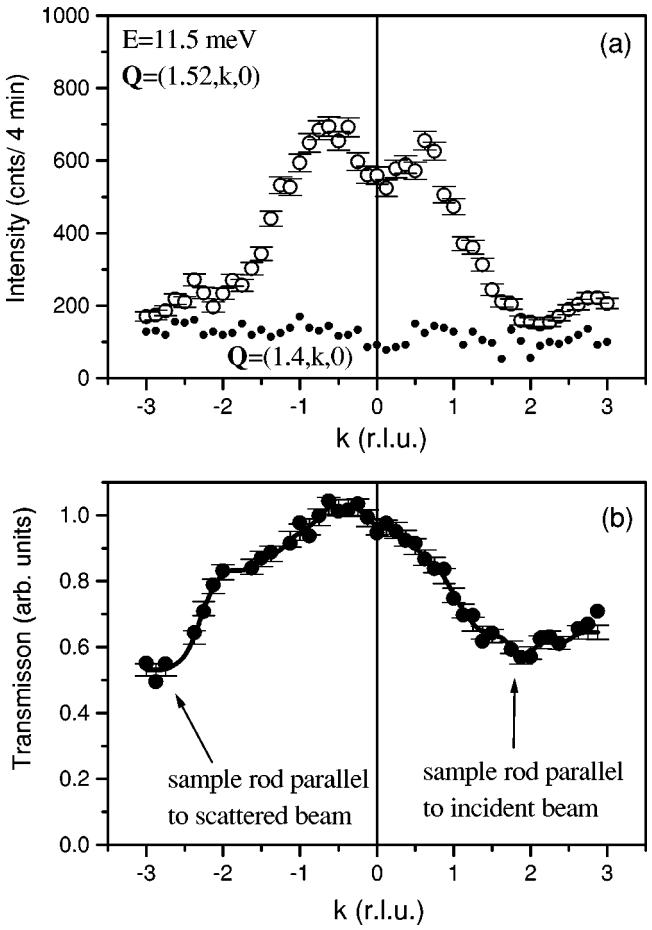

FIG. 8. Measuring the transverse modulation of the Haldane-gap excitations intensity: (a) constant-E scan measured in Nd_2BaNiO_5 at $T=55$ K near the 1D AF zone center $h=1.5$ at $\hbar\omega=11.5$ meV (open circles). The background is measured off the 1D AF zone center (solid circles). (b) Transimission curve for the scan shown in panel (a), measured as explained in the text.

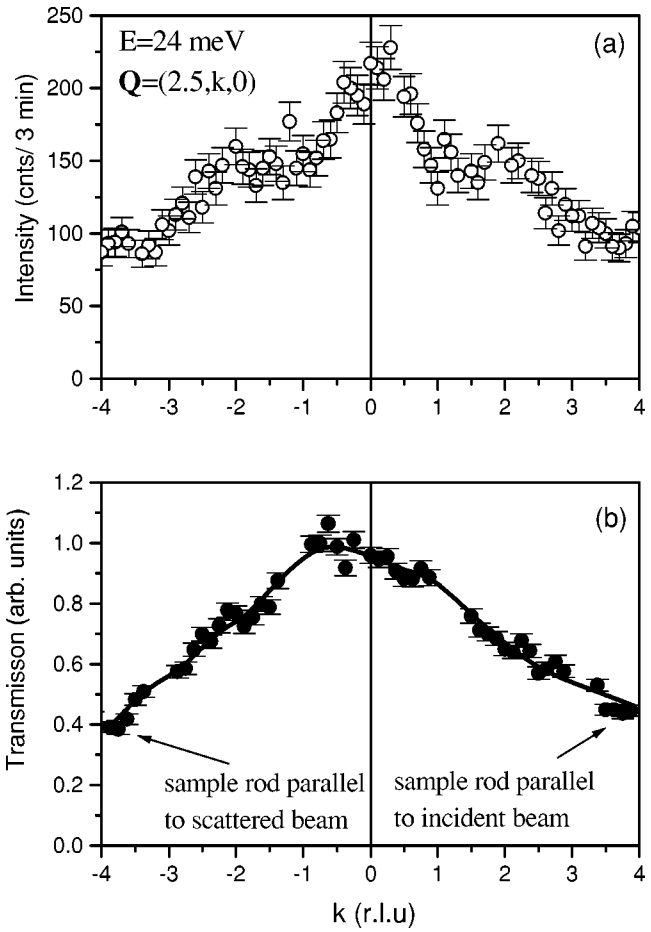

FIG. 9. Measuring the transverse modulation of the 25 meV excitation intensity: (a) constant-E scan measured in Nd_2BaNiO_5 at $T=55$ K near the 1D AF zone center $h=2.5$ at $\hbar\omega=25$ meV. (b) Transmission curve for the scan shown in panel (a), measured as explained in the text.

proportional to the effective transmission coefficient. Typical measured transmission curves are shown in Figs. 8(b) and 9(b). A few Bragg reflections were accidentally picked up in these elastic scans, and the corresponding points were removed from the data sets shown. In Figs. 8(b) and 9(b) arrows indicate geometries of minimum transmission, realized when the sample rods are parallel to the incident or the scattered beams. The measured transmission coefficients were used to scale the measured const-E scans point by point. The resulting corrected data are plotted in Figs. 10 and 11.

Figure 10 shows transmission-corrected k scans taken at the Haldane-gap energy, near two 1D AF zone centers $h=1.5$ and $h=2.5$. The intensity falloff at large $|k|$ is mostly due to focusing and to the effect of magnetic form factors. On top of this falloff, a periodic intensity modulation is clearly seen. The data can be rather well fit to Eq. (7) convoluted with the spectrometer resolution function. The fits are shown in solid lines in Fig. 10 and correspond to $A_H=-0.19(0.02)$. This value is in good agreement with $A_H=-0.17$, obtained from the analysis of constant-Q scans described above.

Figure 11(b) shows that near the 1D AF zone center the intensity of the 25 meV CF mode is modulated as well, in antiphase with that of the Haldane branch. The data can be fit to Eq. (9), assuming $A_2=0.28(0.05)$ [solid line in Fig. 11(b)]. Note that this value is less than a half of that deduced from the analysis of constant-Q scans at the same temperature ($A_2=0.72$). This discrepancy is easily understood. Even at 25 meV energy transfer the Haldane-gap excitations contribute to inelastic scattering, thanks to their steep dispersion along the chain axis that produces long ''tails'' on the high-energy side of the peak in constant-Q scans. The contribution of these tails was not taken into account in the analysis of the wide-range const-E scan shown in Fig. 11(b), but was included in the global fit to constant-Q scans. Our previous estimate for A_2 should thus be considered more accurate.

An important result is that away from the 1D AF zone center, at $h=2.25$, the 25 meV mode shows no oscillations of intensity [Fig. 11(a)]. To within experimental error the measured k dependence can be explained by the Nd form factor alone (solid line). This observation supports the notion that intensity oscillations result from a mixing between CF and Haldane-gap excitations. Away from the 1D AF zone-center Ni-chain modes occur at very-high-energy transfers and therefore do not interact with the dispersionless CF branch.

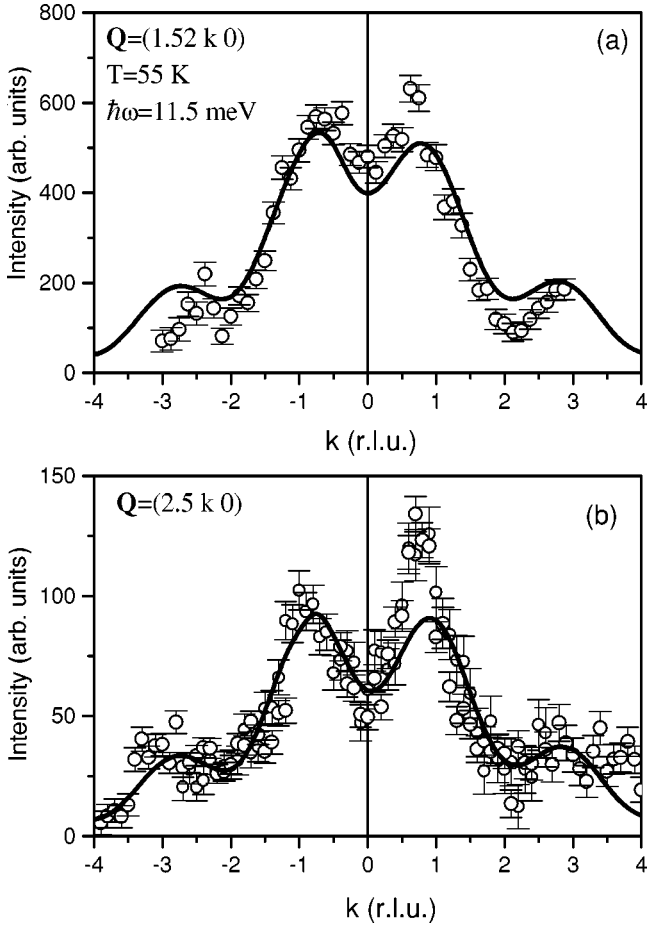

FIG. 10. Transverse modulation of the Haldane-gap excitations intensity: constant-E scans measured in Nd_2BaNiO_5 at $T=55$ K near the 1D AF zone centers $h=1.5$ (a) and $h=2.5$ (b) at $\hbar\omega=11.5$ meV (symbols). The measured intensity has been corrected for absorbtion and the measured background has been subtracted. Solid lines are fits to a model cross section, as described in the text.

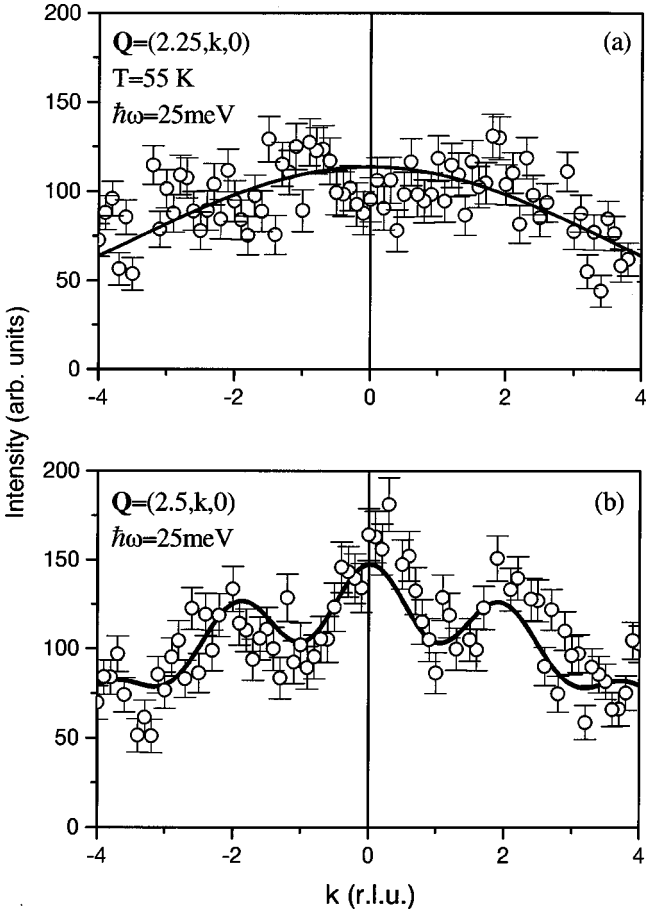

FIG. 11. Transverse modulation of the 25 meV excitation intensity: constant-E scans measured in Nd_2BaNiO_5 at $T=55$ K away from (a) and close to (b) the 1D AF zone center $h=2.5$ at $\hbar\omega=25$ meV (symbols). The measured intensity has been corrected for absorbtion and the measured background has been subtracted. Solid lines are fits to a model cross section, as described in the text.

4. Previous data analysis procedures revised

The discovery of a substantial variation of the intensity in the CF excitations raises concerns about the procedure used to analyze the inelastic data for Nd_2BaNiO_5 in Refs. 6 and 7. In these studies the CF ''background'' was measured away from the 1D AF zone-centers, where the Haldane modes are not seen. The background was then subtracted point by point from the ''signal'' scans measured at the 1D AF zone center. It was assumed that such background-subtracted scans are a good measure of inelastic scattering originating from the Ni chains alone. We now understand that this approach is, in principle, not valid. Although CF excitations are almost dispersionless, their intensity in the ''background'' scans will not necessarily match that in the ''signal'' scans. According to the theoretical model described below, the procedure can only be applied at $k=(2n+1)/2$, $h=(2m+1)/2$ (m, n integer), where there is no mixing between Ni-chain and Nd-single-ion excitations. The data analysis employed in Ref. 7, where measurements were performed at $\boldsymbol{Q}=(1.5,0.5,0)$, is thus fully appropriate. In Ref. 6, on the other hand, the data were taken at $k=0$, and the background subtraction may, in principle, have produced systematic errors. It appears, however, that point-by-point background subtraction is a fairly reliable way to determine the Haldane-gap *energy* at any transverse wave vector. Indeed, in Ref. 6 all scans were taken below 25 meV energy transfer, and thus include only the 18 meV CF excitation. This mode, as we now know, is in fact flat. The main results of Ref. 6 pertain to the temperature dependence of the Haldane gap, which occurs even below 18 meV in the studied temperature range, and are totally valid.

C. Dispersion along the chain axis

The mixing between the Haldane-gap and 24 meV CF modes should be most prominent at points of reciprocal space where the two excitations have similar energies. While the CF excitation is practically dispersionless, the Haldane branch has a steep dispersion along the chain axis, and can be expected to anticross with the 24 meV branch rather close to the 1D AF zone center. To investigate this phenomenon we measured the intensity of inelastic neutron scattering from Nd_2BaNiO_5 on a grid of points in h-E space at $k=0.5$, $h=1.5$–1.8, at $T=55$ K. The result of this measurement is summarized in the grayscale-contour plot in Fig. 12. The circles and squares show the positions of peaks seen when the data are broken up into a collection of constant-Q and constant-E scans, respectively. The most prominent fea-

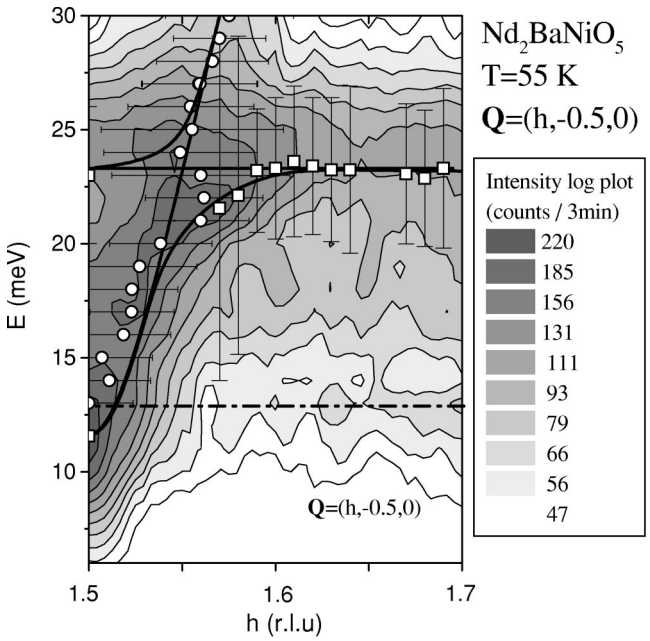

FIG. 12. Logarithmic contour plot of inelastic neutron scattering intensity measured in Nd_2BaNiO_5 at $T=55$ K near the 1D AF zone center $h=1.5$. Circles and squares show peak positions as they appear in constant-E and constant-Q scans, respectively. The bars are peak widths at half height. Solids lines are guides for the eye. Dashed lines represent the dispersion relation expected for the Haldane excitations (parabola) and 25 meV CF mode (straight line) in the absence of mode coupling. The dash-dotted line shows the position of what seems to be a weak, previously unobserved CF excitation.

ture of the spectrum is an anticrossing at the point of intersection of the flat 24 meV CF mode and the parabolic Haldane branch. The solid lines are guides for the eye that emphasize this effect. The anticrossing gap $2\delta E$ can be estimated to be roughly 4 meV. Note that there is no evidence of anticrossing of the Haldane and 18 meV CF branches.

A much less significant feature that is barely seen within the statistics of the measurement is what appears to be a new dispersionless mode at $\hbar\omega\approx 12$ meV (dash-dotted line in Fig. 12). In the single-crystal sample it appears much weaker than the the Haldane mode, but nevertheless may account for the ''shoulder'' seen in powder samples at $T=16.75$ K, as discussed previously. This feature is substantially weaker than the other two CF excitations, and we shall disregard it in the following analysis.

IV. THEORY

It is rather interesting that in Nd_2BaNiO_5 the pronounced transverse modulation of intensity in the Ni-chain and CF excitations is *not* accompanied by any significant transverse dispersion. If we were dealing with a one-component system, e.g., *directly coupled* chains, a narrow bandwidth along a given direction would automatically result in only a weak periodicity in the structure factor. For magnetic excitations in a Bravais crystal, this follows from the sum rule for the first moment of the magnetic dynamic structure factor $S(q,\omega)$.[16] The strong modulation and lack of dispersion in Nd_2BaNiO_5 must therefore be an interference effect that involves both Ni and Nd magnetic degrees of freedom. In the following sections we shall demonstrate that this mixing can be qualitatively accounted for by a simple random-phase-approximation (RPA) model for Ni-R interactions.

A. Bare susceptibilities

1. Ni chains

The first step in the RPA analysis is to determine the bare (noninteracting) dynamic susceptibilities for the Ni and Nd sublattices. For the Haldane spin chains in the vicinity of the 1D AF zone center $q_\parallel=\pi$ we can safely use the single-mode approximation[17–19]

$$\chi^{(0)}_{\mathrm{Ni}}(\boldsymbol{Q},\omega)=\frac{1-\cos Q_\parallel a}{2}\,\frac{Zv}{\Delta^2+v^2\sin^2(Q_\parallel a)-(\hbar\omega+i\epsilon)^2}. \tag{13}$$

In this formula $Q_\parallel$ is the projection of the momentum transfer $\boldsymbol{Q}$ onto the chain axis, v is the spin wave velocity in the chains, $v\approx 6.07\Delta$, and $Z\approx 1.26$ (Ref. 15). It is easily verified that for scattering vectors close to the 1D AF zone center Eq. (2) used to fit the the inelastic scans coincides with the imaginary part of Eq. (13) in the limit $\epsilon\to 0$. In the magnetically ordered state, i.e., in the presence of an effective mean field $\boldsymbol{H}_{eff}$, Eq. (13) can still be utilized. However, the corresponding gap energies for the three components of the Haldane triplet will be modified by $\boldsymbol{H}_{eff}$, as discussed in Refs. 9, 10, 20, and 6.

2. Rare earth ions

For the rare earth subsystem the bare single-ion susceptibility cannot be written down so easily, as the exact electronic configuration of R^{3+} in R_2BaNiO_5 has not been calculated to date. When we were concerned with the mechanism of magnetic ordering in Nd_2BaNiO_5 in Refs.9 and 6, we were dealing with the *static* susceptibility of the rare earths. For Nd^{3+} at low temperatures the static susceptibility can be, to a good approximation, attributed to the lowest-energy Kramers doublet and written as a $S=1/2$ Brillouin function. For our present purpose of studying the *dynamic* coupling of Nd and Ni subsystems we are interested in the *dynamic* susceptibility of Nd^{3+} at frequencies comparable to the Haldane-gap energy. In the paramagnetic phase the contribution to χ_{Nd} from the ground state doublet is *purely elastic* and can thus be totally ignored in the RPA calculation. At $T>T_{\mathrm{N}}$ we therefore only need to consider the contribution of transitions between the ground-state of the ion and higher-energy crystal-field levels. In the ordered phase, we also have to take into account single-ion transitions within the ground-state doublet, which becomes split by the mean exchange field.[6] As a first step, we shall consider only one excited level of Nd^{3+}, at energy E. Transitions from the ground state to the excited state produce the following term in Nd single-ion susceptibility:

$$\chi^{(0)}_{\mathrm{Nd}}(\omega)=M^2\frac{E}{E^2-(\hbar\omega+i\epsilon)^2}R(T). \tag{14}$$

In this formula M is the matrix element of the magnetic moment operator between the ground state and the excited

state. $R(T)$ is the temperature renormalization factor defined as the difference in populations of the excited and ground states. To simplify our qualitative analysis, in Eq. (14) we have ignored any terms that are off diagonal in spin projection indexes, and the above formula thus applies to a particular selected channel of spin polarization.

B. Interaction geometry

Let us now consider the geometry of Ni-Nd exchange interactions (Fig. 1). The antiferromagnetic coupling denoted by J_1 stabilizes the magnetic structure seen in the low-temperature phase, and is responsible for the staggered mean field at $T<T_N$. As is often the case in body-centered crystals, the coupling J_2 is geometrically frustrated. Indeed, it links a single R^{3+} moment to two subsequent Ni^{2+} spins in the chains that are strongly coupled antiferromagnetically between themselves. As a result, at the MF level J_2 plays no role in long-range ordering. Below we shall arbitrarily assume that the exchange matrix is diagonal in spin projection indexes. In the body-centered structure, with two R sites per every Ni, we have to consider six magnetic ions: Ni(1) at (0.5,0.5,0), Ni(2) at (0,0,0.5), Nd(3) at (0.5,0,d), Nd(4) at (0.5,0,$-$d), Nd(5) at (0,0.5,d$-$0.5), and Nd(6) at (0,0.5, $-$[d$-$0.5]), where $d\approx 0.2$. For the RPA calculation we need the Fourier transform of the exchange matrix in this basis set:

$$J_\perp(\boldsymbol{Q})=\begin{pmatrix} 0 & 0 & J_1(\boldsymbol{Q}) & J_1^*(\boldsymbol{Q}) & J_2(\boldsymbol{Q}) & J_2^*(\boldsymbol{Q}) \\ 0 & 0 & J_2(\boldsymbol{Q}) & J_2^*(\boldsymbol{Q}) & J_1(\boldsymbol{Q}) & J_1^*(\boldsymbol{Q}) \\ J_1^*(\boldsymbol{Q}) & J_2^*(\boldsymbol{Q}) & 0 & 0 & 0 & 0 \\ J_1(\boldsymbol{Q}) & J_2(\boldsymbol{Q}) & 0 & 0 & 0 & 0 \\ J_2^*(\boldsymbol{Q}) & J_1^*(\boldsymbol{Q}) & 0 & 0 & 0 & 0 \\ J_2(\boldsymbol{Q}) & J_1(\boldsymbol{Q}) & 0 & 0 & 0 & 0 \end{pmatrix}, \tag{15}$$

$$J_1(\boldsymbol{Q})=2J_1\cos(\pi k)\exp(2\pi i l d), \tag{16}$$

$$J_2(\boldsymbol{Q})=2J_2\cos(\pi h)\exp[2\pi i l(d-0.5)]. \tag{17}$$

One readily sees that, in the reciprocal-space planes $(h,2n+1/2,l)$ (n integer), J_1 interactions cancel out and can be ignored. A similar cancellation occurs for J_2 in the $((2n+1)/2,k,l)$ (n integer) planes. These cancellations result from interaction topology, and do not rely on any of our assumptions regarding the bare susceptibilities.

C. RPA susceptibility

The assumptions made above bring us to a simple mode-coupling problem in each channel of spin polarization. The RPA susceptibility matrix is written as $\chi^{\mathrm{RPA}}(\boldsymbol{Q},\omega)=[1+\chi^0(\boldsymbol{Q},\omega)J(\boldsymbol{Q})]^{-1}\chi^0(\boldsymbol{Q},\omega)$.

1. Dispersion

The dispersion relation is obtained by solving the equation $\det([\chi^{\mathrm{RPA}}]^{-1})=0$. In our case of only one excited Nd state this can easily be done analytically. With six independent atoms we obtain six modes (two of them degenerate):

$$2(\hbar\omega_{1,2})^2=\Delta_{Q_\parallel}^2+E^2\pm\sqrt{(\Delta_{Q_\parallel}^2-E^2)^2+8EM^2Zv\mathcal{J}_+^2},$$

$$2(\hbar\omega_{3,4})^2=\Delta_{Q_\parallel}^2+E^2\pm\sqrt{(\Delta_{Q_\parallel}^2-E^2)^2+8EM^2Zv\mathcal{J}_-^2},$$

$$\hbar\omega_{5,6}=E, \tag{18}$$

where we have introduced the notation $\Delta_{Q_\parallel}^2=\Delta^2+v^2\sin^2(Q_\parallel a)$, and

$$\mathcal{J}_\pm^2=|J_1(\boldsymbol{Q})\pm J_2(\boldsymbol{Q})|^2=4J_1^2\cos^2(\pi k)+4J_2^2\cos^2(\pi h)\pm 16J_1J_2\cos(\pi k)\cos(\pi h)\cos(\pi l). \tag{19}$$

We have implicitly dropped the $(1-\cos Q_\parallel a)/2$ factor in $\chi_{\mathrm{Ni}}^{(0)}$ and the temperature factor R in $\chi_{\mathrm{Nd}}^{(0)}$.

Particularly useful is the linearized version of Eq. (18) which becomes valid in the weak-coupling limit:

$$\hbar\omega_1(\mathbf{Q})=\Delta_{Q_\parallel}-\mathcal{J}_+(\boldsymbol{Q})^2\frac{Zv}{\Delta}\frac{EM^2}{E^2-\Delta_{Q_\parallel}^2},$$

$$\hbar\omega_2(\mathbf{Q})=+\mathcal{J}_+(\boldsymbol{Q})^2\frac{Zv}{\Delta}\frac{EM^2}{E^2-\Delta_{Q_\parallel}^2},$$

$$\hbar\omega_3(\mathbf{Q})=\Delta_{Q_\parallel}-\mathcal{J}_-(\boldsymbol{Q})^2\frac{Zv}{\Delta}\frac{EM_1^2}{E^2-\Delta_{Q_\parallel}^2},$$

$$\hbar\omega_4(\mathbf{Q})=E+\mathcal{J}_-(\boldsymbol{Q})^2\frac{Zv}{\Delta}\frac{EM_1^2}{E^2-\Delta_{Q_\parallel}^2},$$

$$\hbar\omega_{5,6}(\mathbf{Q})=E. \tag{20}$$

The first and third branches can be described as Ni-chain Haldane-gap modes with an admixture of Nd-spin correlations. The second and fourth branches, conversely, are CF excitations with a small component of Ni spins. If the Nd-

single-ion excitation lies above the Haldane branch at a given wave vector, the energy of the Ni-chain mode is pushed down by Ni-Nd interactions, while the CF excitation energy is increased. The reverse is expected in the case of a single-ion excitation inside the Haldane gap. Modes 5 and 6 appear as totally unperturbed single-ion transitions. A very important result is that the transverse dispersion resulting from Ni-*R* interactions is *quadratic* in $\mathcal{J}$ and is thus expected to be very small in the weak-coupling limit.

Also useful for our purposes are values of anticrossing gaps at the point of mode intersection. According to Eqs. (18) these are given by

$$2\,\delta E_{1\leftrightarrow 2}=\mathcal{J}_{+}M\sqrt{\frac{2Zv}{E}},$$

$$2\,\delta E_{3\leftrightarrow 4}=\mathcal{J}_{-}M\sqrt{\frac{2Zv}{E}}, \tag{21}$$

for the two pairs of intersecting same-symmetry branches, respectively. Intersection of branches of different symmetry (1,4) and (2,3) does not lead to an anticrossing effect.

2. Intensity modulation

The inelastic neutron scattering cross section is related to the imaginary part of dynamic susceptibility through the fluctuation-dissipation theorem. To get the actual intensities we also have to take into account the Ni and *R* magnetic form factors $f_{\mathrm{Ni}}(Q)$ and $f_{\mathrm{Nd}}(Q)$:

$$\frac{d\sigma}{d\Omega}\propto[f_{\mathrm{Ni}}(Q)\;\; f_{\mathrm{Ni}}(Q)\;\; f_{\mathrm{Nd}}(Q)\;\; f_{\mathrm{Nd}}(Q)\;\; f_{\mathrm{Nd}}(Q)\;\; f_{\mathrm{Nd}}(Q)]\chi''(\boldsymbol{Q},\omega)\begin{pmatrix} f_{\mathrm{Ni}}(Q)\\ f_{\mathrm{Ni}}(Q)\\ f_{\mathrm{Nd}}(Q)\\ f_{\mathrm{Nd}}(Q)\\ f_{\mathrm{Nd}}(Q)\\ f_{\mathrm{Nd}}(Q)\end{pmatrix}. \tag{22}$$

The task of calculating the total $\chi''(\boldsymbol{Q},\omega)$ is greatly simplified in the weak-coupling limit, where one can write $\chi^{\mathrm{RPA}}(\boldsymbol{Q},\omega)\approx[1-\chi^{0}(\boldsymbol{Q},\omega)J(\boldsymbol{Q})]\chi^{0}(\boldsymbol{Q},\omega)$. At this level of approximation the two Haldane excitations (modes 1 and 3) are not distinguished. The same applies to CF modes 2, 4, 5, and 6. For the sum of the partial cross sections of the Haldane modes a straightforward yet somewhat tedious calculation gives

$$\frac{d\sigma_{1+3}}{d\Omega}\propto\frac{Zv}{\Delta_{Q_\parallel}}\left(f_{\mathrm{Ni}}(Q)^2-4f_{\mathrm{Ni}}(Q)f_{\mathrm{Nd}}(Q)\frac{EM^2}{E^2-\Delta_{Q_\parallel}^2}\times\mathrm{Re}[J_1(\boldsymbol{Q})+J_2(\boldsymbol{Q})]\right). \tag{23}$$

Similarly, for the single-ion modes,

$$\frac{d\sigma_{2+4}}{d\Omega}\propto 2M^2\left(f_{\mathrm{Nd}}(Q)^2+4f_{\mathrm{Ni}}(Q)f_{\mathrm{Nd}}(Q)\frac{Zv}{E^2-\Delta_{Q_\parallel}^2}\times\mathrm{Re}[J_1(\boldsymbol{Q})+J_2(\boldsymbol{Q})]\right). \tag{24}$$

One readily sees that, unlike the corrections to the dispersion relation, corrections to mode intensities are *linear* in J_1 and J_2 and can be substantial. The linear form of Eqs. (20), (23), and (24) enables a straightforward generalization to the case of several Nd-single-ion transitions.

3. Results for the 1D AF zone center

The expressions for the dynamic structure factor can be further simplified for scattering vectors in $((2n+1)/2,k,l)$ (n integer) reciprocal-space planes, where most of the neutron data were collected. Here the effect of J_2 is totally canceled, and there are only three branches in the spectrum: the Haldane branch (labeled ''H''), a CF branch that interacts with the Ni-chain excitations (''CF''), and the unperturbed CF transition (''CF_0''). Using Eq. (22) on the exact (rather than linearized) RPA susceptibility matrix and truncating the result to the first order in J_1, we obtain

$$\frac{d\sigma_{\mathrm{H}}}{d\Omega}\propto\frac{Zv}{\Delta_{Q_\parallel}}\left(f_{\mathrm{Ni}}(Q)^2-8J_1f_{\mathrm{Ni}}(Q)f_{\mathrm{Nd}}(Q)\times\frac{EM^2}{E^2-\Delta_{Q_\parallel}^2}\cos(\pi k)\cos(2\pi ld)\right), \tag{25}$$

$$\frac{d\sigma_{\mathrm{CF}}}{d\Omega}\propto 2M^2\left(f_{\mathrm{Nd}}(Q)^2[1+\cos(4\pi ld)]+8J_1f_{\mathrm{Ni}}(Q)f_{\mathrm{Nd}}(Q)\frac{Zv}{E^2-\Delta_{Q_\parallel}^2}\cos(\pi k)\cos(2\pi ld)\right), \tag{26}$$

$$\frac{d\sigma_{\mathrm{CF}_0}}{d\Omega}\propto 2M^2f_{\mathrm{Nd}}(Q)^2[1-\cos(4\pi ld)]. \tag{27}$$

The intensity of all three modes becomes modulated. The period of modulation along the b axis is exactly $2b^*$, while that along c is incommensurate with the lattice. For the reciprocal-space rods $((2n+1)/2,k,0)$ (n integer) the mode CF_0 vanishes and only two branches remain. For the purpose of convenience we shall also rewrite Eqs. (20) for the $((2n+1)/2,k,l)$ (n integer) planes:

$$\hbar\omega_{\mathrm{H}}(\mathbf{Q})=\Delta_{Q_\parallel}-4J_1(\boldsymbol{Q})^2\frac{Zv}{\Delta}\frac{EM^2}{E^2-\Delta_{Q_\parallel}^2}\cos^2(\pi k), \quad (28)$$

$$\hbar\omega_{\mathrm{CF}}(\mathbf{Q})=\Delta_1+4J_1(\boldsymbol{Q})^2\frac{Zv}{\Delta}\frac{EM^2}{E^2-\Delta_{Q_\parallel}^2}\cos^2(\pi k), \quad (29)$$

$$\hbar\omega_{\mathrm{CF}_0}(\mathbf{Q})=E. \quad (30)$$

As noted previously, the magnitude of transverse dispersion is proportional to J_1^2.

We cannot expect the model described above to be quantitatively valid for any real R_2BaNiO_5 system. Its main limitation is that it assumes the exchange matrix and the matrix elements of momentum between the rare earth ground and excited states to be simultaneously diagonal in spin projection indexes. In the R_2BaNiO_5 structure, the rare earth sites have a very low symmetry and the bare susceptibility and exchange matrixes are bound to be rather complex. We can, however, expect the model to make qualitatively correct predictions regarding the periods and signs of modulations of excitation intensities and energies.

4. Paramagnetic phase

For Nd_2BaNiO_5 we should distinguish two regimes. At $T>T_N$, at energy transfers below 30 meV, only the 18 meV and the 24 meV Nd modes will mix with the Haldane-gap excitations. Experimentally, the 18 meV transition appears totally decoupled from the Ni chains. This is most likely due to its particular polarization and the actual form of the exchange tensors. For example, if the 18 meV excitation were polarized along the x axis and J_1^{xx} is zero, then no mixing would occur. The 24 meV excitation is thus the only one that mixes with the Haldane branches, producing the observed modulations.

The RPA model, oversimplified as it is, justifies the use of Eqs. (6)–(12) in fitting the inelastic neutron scattering data. From this analysis we can even extract some useful quantitative information. According to Eqs. (28) and (25), the ratio $B_{\mathrm{H}}/A_{\mathrm{H}}$ [see Eqs. (7) and (10)] is *independent* of any parameters of the rare earth ions:

$$B_{\mathrm{H}}/A_{\mathrm{H}}=\frac{Zv}{2\Delta}J_1. \quad (31)$$

This is a robust result that allows us to obtain at least an order-of-magnitude estimate for J_1, without making any assumptions regarding Nd^{3+}. For an isolated Haldane spin chain $Zv\approx 7.6\Delta$, so $B_{\mathrm{H}}/A_{\mathrm{H}}\approx 3.8J_1$. From the $T=55$ K experimental values $A=-0.17$ meV and $B=-0.19$ we get $J_1\approx 0.3$ meV. We can compare this value to the MF coupling α for Nd_2BaNiO_5 that we obtained in Refs. 9 and 6. Indeed, $J_\perp$ should be related to α through $J_1M^{(Ni)}M^{(Nd)}=\alpha/2$, which gives $J_1\approx 0.5$ meV, in reasonable agreement with our new estimate.

A more crude estimate can also be obtained for J_2, which in our model is the only possible source of the observed anticrossing between the Haldane and 24 meV CF branches (Fig. 12). Indeed, at $k=0.5$ where these data were taken the effect of J_1 is canceled, according to Eq. (16). Experimentally, the anticrossing is about 4 meV. From Eq. (21) we get $J_2M_1\approx 0.8$ meV. The 24 meV CF mode and the Haldane excitation are of comparable intensity, and based on Eqs. (25) and (26) we can assume that $M^2\sim Zv/\Delta$, which gives $M\sim 3$. This gives us an estimate for J_2: of the order of 0.2 meV. This is a rather reasonable value for a rare-earth–transition-metal superexchange bond.

5. Ordered state

In the magnetically ordered phase an additional Nd-centered excitation, namely, the 4 meV Ising-like spin wave that appears below T_N (see $T=16.5$ K data in Fig. 2), will also mix with the Ni-chain modes. Being inside the Haldane gap, it will produce intensity and energy modulations that are opposite to those resulting from the mixing with the high-energy 24 meV branch. Intensity oscillations in the Haldane branch will thus be reduced, in agreement with our experimental findings. As observed in previous studies, the intensity of the peak corresponding to Haldane excitations is reduced by almost a factor of 2. This results from the suppression of the b-axis-polarized Haldane excitation (longitudinal mode) in the ordered state.[7] In the framework of the RPA model, a decrease of spectral weight in the Haldane branches inevitably leads to a smaller interference effect in the CF mode. Such a reduction of intensity modulation in the ordered state is indeed observed experimentally for the 24 meV excitation (see Table I).

V. SUMMARY

We have demonstrated that local excitations associated with magnetic rare earth ions play an important role in the magnetism of R_2BaNiO_5 quantum antiferromagnets. Even in the 1D (paramagnetic) phase there are substantial *dynamic* interactions between quantum spin chains and the rare earth subsystem. This phenomenon can be qualitatively accounted for by a simple chain-RPA model. Not having more detailed information on the electronic states of the rare earth ions, using this model for a quantitative analysis of the data is obviously a leap of faith. It does, however, produce reasonable order-of-magnitude estimates for Ni-Nd coupling constants.

At any temperature the Haldane-gap modes cannot be considered as purely Ni excitations, and their interference with Nd-single-ion modes is substantial. Despite that, the Haldane-gap *energy* is practically the same as in *isolated* chains in a *static* mean exchange field, and the transverse dispersion is very small. The static staggered exchange field model is thus fully justified for Nd_2BaNiO_5, as are all our previous results for the temperature (staggered field) dependence of the Haldane gap.

ACKNOWLEDGMENTS

The authors would like to thank P. Dai, J. Zarestky, B. Taylor, and R. Rothe for expert technical assistance. Work at BNL was carried out under Contract No. DE-AC02-98CH10886, Division of Material Science, U.S. Department of Energy. Oak Ridge National Laboratory is managed for the U.S. DOE by Lockheed Martin Energy Research Corporation under Contract No. DE-AC05-96OR22464.

[1] For a recent review, see A. Zheludev, Neutron News **10**, 16 (1999).
[2] J. Darriet and L.P. Regnault, Solid State Commun. **86**, 409 (1993); T. Yokoo, T. Sakaguchi, K. Kakurai, and J. Akimitsu, J. Phys. Soc. Jpn. **64**, 3651 (1995); G. Xu *et al.*, Phys. Rev. B **54**, R6827 (1996).
[3] A. Zheludev, J.M. Tranquada, T. Vogt, and D.J. Buttrey, Europhys. Lett. **35**, 385 (1996); Phys. Rev. B **54**, 6437 (1996).
[4] A. Zheludev, J.M. Tranquada, T. Vogt, and D.J. Buttrey, Phys. Rev. B **54**, 7216 (1996).
[5] T. Yokoo, A. Zheludev, M. Nakamura, and J. Akimitsu, Phys. Rev. B **55**, 11 516 (1997).
[6] T. Yokoo, S. Raymond, A. Zheludev, S. Maslov, E. Ressouche, I. Zaliznyak, R. Erwin, M. Nakamura, and J. Akimitsu, Phys. Rev. B **58**, 14 424 (1998).
[7] S. Raymond, T. Yokoo, A. Zheludev, S.E. Nagler, A. Wildes, and J. Akimitsu, Phys. Rev. Lett. **82**, 2382 (1999).
[8] E. García-Matres *et al.*, J. Solid State Chem. **103**, 322 (1993); **149**, 363 (1995).
[9] A. Zheludev *et al.*, Phys. Rev. Lett. **80**, 3630 (1998).
[10] S. Maslov and A. Zheludev, Phys. Rev. Lett. **80**, 5786 (1998).
[11] J. Lou, X. Dai, S. Quin, Z. Su, and L. Yu, Phys. Rev. B **60**, 52 (1999).
[12] I. Bose and E. Chattopadhyay, cond-mat/9904311 (unpublished).
[13] E. García-Matres *et al.*, J. Solid State Chem. **103**, 322 (1993).
[14] V. Sachan, D.J. Buttrey, J.M. Tranquada, and G. Shirane, Phys. Rev. B **49**, 9658 (1994).
[15] E.S. Sorensen and I. Affleck, Phys. Rev. B **49**, 15 771 (1994).
[16] G. Muller, H. Thomas, M.W. Puga, and H. Beck, J. Phys. C **14**, 3399 (1981).
[17] D.P. Arovas, A. Auerbach, and F.D.M. Haldane, Phys. Rev. Lett. **60**, 531 (1988).
[18] G. Muller, H. Thomas, M.W. Puga, and H. Beck, J. Phys. C **14**, 3399 (1981).
[19] S. Ma, C. Broholm, D.H. Reich, B.J. Sternlieb, and R.W. Erwin, Phys. Rev. Lett. **69**, 3571 (1992).
[20] S. Maslov and A. Zheludev, Phys. Rev. B **57**, 68 (1998).